

Experimental Evaluation of the Reconfigurable Photodetector for Blind Interference Alignment in Visible Light Communications

Máximo Morales-Céspedes, Ahmad Adnan Quidan, Ana García Armada

Department of Signal Theory and Communications. University Carlos III of Madrid, Leganés, Spain

Email: {maximo, ahmadq, agarcia}@tsc.uc3m.es

Abstract—Visible light communications (VLC) have been proposed as an alternative to the radio-frequency (RF) communications because of the huge unlicensed bandwidth available and a low cost implementation. In this context, one of the most interesting applications of VLC is their use in vehicular communications using the headlights of trucks, cars or motorbikes. However, the vehicular communications are subject to blocking from other elements of the network or weather effects such as rain or fog. To solve these issues we propose the use of multi-photodiode receivers following an angle diversity distribution. In particular, in this work we focus on a configuration that considers a single signal processing chain connected to the set of photodiodes through a selector referred to as reconfigurable photodetector. First, we obtain the experimental evaluation of the optical channel considering high-power optical transmitters and several angle diversity configurations. After that, an offline evaluation of the blind interference alignment (BIA) scheme is carried out in comparison with a diversity scheme such as maximum ratio combining (MRC).

I. INTRODUCTION

During the recent years, visible light communications (VLC) have been proposed as an alternative to the existing radio-frequency (RF) based communications [1]. In this sense, given some features such as the huge unlicensed bandwidth available in the optical domain, avoiding the interference with the RF communications, the high energy efficiency or the low cost implementation of the optical devices, VLC result suitable for vehicular communications [2].

In this context, the use of VLC applications in vehicular communications involves to solve some challenges. First, it must provide enough robustness to the noise, blocking effects and weather conditions within a wide distance range while providing low latency [3]. Moreover, due to the inherent features of the vehicular communications the solution to these issues has to be resilient to high mobility scenarios [4]. On the other hand, taking into consideration the increasing amount of information that the vehicles generate, future vehicular communications require high data rates. In this sense, optical MIMO solutions have been proposed. However, most of the MIMO schemes that achieve an increase of the data rate are based on knowledge of the channel state information at the transmitter (CSIT). For indoor VLC the knowledge of the CSIT can be easily achieved considering quasi-static users,

however, it results extremely difficult to obtain in vehicular communications. Furthermore, the distinct sources of optical transmitters such as headlights, traffic lights or street lights naturally generate a heterogeneous network, in which these MIMO schemes result challenging to implement.

To avoid the effects of the interference among distinct optical transmitters while providing a robust link, the use of angle diversity (AD) receivers has been proposed in [5]. Basically, the AD receivers are composed of several photodiodes each pointing to a distinct orientation. Notice that the arrangement of photodiodes for AD receivers usually follows a geometrical pattern, e.g., pyramidal or hemispherical, as described in [6]. Taking into consideration the architecture of the AD receivers the interference is typically avoided through diversity schemes, e.g., maximum ratio combining (MRC) [5]. However, these diversity schemes are subject to obtaining the weights that maximize the sum of the signal-to-noise ratio (SNR), which increases the complexity of the receiver. Moreover, the achievable user rate for diversity schemes is usually limited by the interference instead of by SNR.

A novel transmission scheme that can potentially solve these issues referred to as blind interference alignment (BIA) is proposed in [7]. Basically, BIA exploits the channel correlations among the users to generate multiplexing gain, also known as degrees of freedom (DoF), without the need for CSIT. Although the implementation of BIA in RF is challenging, in [8] it is shown that BIA-based schemes result suitable to VLC systems. However, the implementation of BIA schemes in VLC requires to employ an AD receiver referred to as reconfigurable photodetector in which the set of photodiodes are connected to a single signal processing chain through a selector. In this sense, the key idea of the reconfigurable photodetector is to provide to each user a set of channel responses linearly independent among them.

In this work, we present an experimental evaluation of the reconfigurable photodetector. First, we evaluate the channel response for this receiver architecture. In this sense, we consider distinct models of photodiodes to determine the effects of the field-of-view (FoV) in the reconfigurable photodetector. After that, we present the offline evaluation of the user rate considering the obtained channel for BIA and diversity schemes. It is shown that the reconfigurable photodetector requires photodiodes with a narrow FoV in order to obtain linearly independent channel responses. Furthermore, the performance

	1	2	3
$k=1$	$\mathbf{h}^{[1]}(1)$	$\mathbf{h}^{[1]}(2)$	$\mathbf{h}^{[1]}(1)$
$k=2$	$\mathbf{h}^{[2]}(1)$	$\mathbf{h}^{[2]}(1)$	$\mathbf{h}^{[2]}(2)$

Fig. 1. BIA supersymbol for the considered case. $L = 2$, $K = 2$. Each color represents a preset mode of the photodiode.

of BIA tends to be the same as the achieved for totally linearly independent channel responses when the orientation of the photodiodes is properly selected.

II. SYSTEM MODEL

We consider a VLC network composed of L , $l = \{1, \dots, L\}$, optical transmitters that send information to K , $k = \{1, \dots, K\}$, users equipped with a reconfigurable photodetector each. Basically, a reconfigurable photodetector provides M , $m = \{1, \dots, M\}$, distinct linearly independent channel responses each referred to as a preset mode. Moreover, each receiver is only equipped with a single signal processing chain so that only a specific preset mode can be selected at time n . The signal transmitted by the L optical transmitters at time n can be written in a vector form as $\mathbf{x}[n] = [x_1 \dots x_L] \in \mathbb{R}_+^{L \times 1}$, where x_l is the signal of the transmitter l . Thus, the signal received by the user k corresponding to the preset mode m at time n can be written as

$$y^{[k]}[n] = \mathbf{h}^{[k]} \left(m^{[k]}[n] \right)^T \mathbf{x}[n] + z^{[k]}[n], \quad (1)$$

where $\mathbf{h}^{[k]} \in \mathbb{R}^{L \times 1}$ is the channel between the L transmitters and the user k associated to the preset mode m and $z^{[k]}$ is additive white gaussian noise (AWGN).

III. BLIND INTERFERENCE ALIGNMENT

In this section we present a brief overview of the BIA scheme for the broadcast channel (BC) [7]. For illustrative purposes we focus on the $L = 2$ and $K = 2$ case, which corresponds to two headlights transmitting to $K = 2$ vehicular receivers. The BIA scheme considers a switching pattern of preset modes as is shown in Fig. 1, which is referred to as supersymbol from now on. For this supersymbol, the transmitted signal is

$$\mathbf{X} = \begin{bmatrix} \mathbf{x}[1] \\ \mathbf{x}[2] \\ \mathbf{x}[3] \end{bmatrix} = \begin{bmatrix} \mathbf{I}_2 \\ \mathbf{I}_2 \\ \mathbf{0}_2 \end{bmatrix} \mathbf{u}^{[1]} + \begin{bmatrix} \mathbf{I}_2 \\ \mathbf{0}_2 \\ \mathbf{I}_2 \end{bmatrix} \mathbf{u}^{[2]} \quad (2)$$

where $\mathbf{u}^{[k]} = [u_1^{[k]}, u_2^{[k]}]^T$ is the symbol intended to the user k and $u_l^{[k]}$ is the symbol corresponding to the transmitter l . Notice that no CSIT nor data sharing among transmitters is required to compose the transmitted signal (2).

Focussing on the user 1 the received signal is given by

$$\begin{bmatrix} y^{[1]}[1] \\ y^{[1]}[2] \\ y^{[1]}[3] \end{bmatrix} = \underbrace{\begin{bmatrix} \mathbf{h}^{[1]}(1)^T \\ \mathbf{h}^{[1]}(2)^T \\ \mathbf{0}_{2,1}^T \end{bmatrix}}_{\text{rank}=2} \mathbf{u}^{[1]} + \underbrace{\begin{bmatrix} \mathbf{h}^{[1]}(1)^T \\ \mathbf{0}_{2,1}^T \\ \mathbf{h}^{[1]}(1)^T \end{bmatrix}}_{\text{rank}=1} \mathbf{u}^{[2]} + \begin{bmatrix} z^{[1]}[1] \\ z^{[1]}[2] \\ z^{[1]}[3] \end{bmatrix}. \quad (3)$$

Notice that the desired symbol is contained in a rank-2 matrix while the interference is in a rank-1, i.e., the interference is aligned. Thus, the interference because of transmission of $\mathbf{u}^{[2]}$ can be measured at the third symbol extension and removed from the first symbol extension. Hence, the received signal after interference subtraction is

$$\begin{bmatrix} y^{[1]}[1] - y^{[1]}[3] \\ y^{[1]}[2] \end{bmatrix} = \underbrace{\begin{bmatrix} \mathbf{h}^{[1]}(1)^T \\ \mathbf{h}^{[1]}(2)^T \end{bmatrix}}_{\mathbf{H}^{[1]}} \mathbf{u}^{[1]} + \begin{bmatrix} z^{[1]}[1] - z^{[1]}[3] \\ z^{[1]}[2] \end{bmatrix}. \quad (4)$$

Notice that the user k can decode $\mathbf{u}^{[1]}$ solving the equation system given by (4) subject to noise distortion. Notice that the two symbols contained in $\mathbf{u}^{[1]}$ are only decodable if the entries of the channel matrix $\mathbf{H}^{[1]} = [\mathbf{h}^{[1]}(1)^T, \mathbf{h}^{[1]}(2)^T]$, i.e., the channel responses associated to each preset mode, are linearly independent.

For the considered case, the user 2 can follow a similar procedure measuring the interference during the second symbol extension. Therefore, each user achieves $\frac{2}{3}$ DoF for the proposed BIA scheme. It is interesting to remark that orthogonal resource allocation divides 1 DoF between both users, e.g., considering a time division scheme.

The general BIA scheme for the BC is described in detail in [7]. It is shown that BIA is DoF-optimal in absence of CSIT. Focussing on the achievable rate, the rate of the user k is given by

$$R_{\text{BIA}}^{[k]} = \frac{1}{L+K-1} \log_2 \left(\det \left(\mathbf{I}_L + P_{\text{str}} \mathbf{H}^{[k]} \mathbf{H}^{[k]H} \mathbf{R}_z^{-1} \right) \right), \quad (5)$$

where P_{str} is the power allocated to each stream, $\mathbf{H}^{[k]}$ is the channel matrix of the user k given by

$$\mathbf{H}^{[k]} = \begin{bmatrix} \mathbf{h}^{[k]}(1)^T & \dots & \mathbf{h}^{[k]}(M)^T \end{bmatrix}^T, \quad (6)$$

and

$$\mathbf{R}_z = \begin{bmatrix} K \mathbf{I}_{M-1} & 0 \\ 0 & 1 \end{bmatrix} \quad (7)$$

is the noise enhancement matrix because of the interference subtraction. Notice that the user rate depends on providing linearly independent channel responses for each preset mode (see (6)). In other words, the preset modes of the reconfigurable photodetector must maximize $\det(\mathbf{H}^{[k]} \mathbf{H}^{[k]H})$.

IV. SYSTEM SET-UP

A. Transmitter

The signal transmitted in the optical domain must be real and non-negative. Moreover, the output optical power is only linear over a limited drive current within the range $[I_L, I_H]$, where I_L corresponds to the forward current that provides a minimum optical power and I_H is the current from which the output optical power becomes non-linear. Within this range, the output optical power is limited between 0 and P_{\max} . Notice that the VLC system must ensure a constant and sufficient illumination. Thus, we first add a DC bias current denoted as I_{DC} while the transmitted signal varies around I_{DC} . This methodology provides an average optical power P_{avg}

independently of the transmitted signal. Moreover, taking into consideration a practical system, the variations because of signal transmission must generate fluctuations that are non-detectable to the human eye.

In this work, we consider two LED lamps CitiLed Chip-on-Board (CoB) CLU048-1212C4 [9], which can be employed for outdoor illumination or car headlights. A constant forward current $I_{DC} = 200$ mA is considered, which provides an illumination efficiency of 70 lm/W. Furthermore, we consider a signal variation of ± 25 mA with a frequency above 10 KHz to avoid detectable fluctuations to the human eye. At this point, it is interesting to remark that the considered CoB LED lights provide a bandwidth greater than 1 MHz.

B. Optical channel

The VLC channel is composed of a flat and a diffuse component corresponding to the LoS and NLoS propagation, respectively. The diffuse component represents the reflection on walls, floor and ceiling. Notice that this component can provide a considerable contribution in tunnels or other confined structures of the vehicular communications. In the time domain, the optical channel between the transmitter l and the user k given by the preset mode m at time n can be written as

$$\eta_l^{[k]}(m, n) = \eta_{\text{LoS}, l}^{[k]}(m)\delta[n] + \eta_{\text{diff}}[n - \Delta T], \quad (8)$$

where $\eta_{\text{LoS}, l}$ and η_{diff} represent the LoS and NLoS components and ΔT is the delay between the LoS and the NLoS components.

The LoS component is inversely proportional to the square of the distance between the transmitter l and the user k denoted as d_{kl} and the angles of radiation and incidence, which are referred to as $\phi_l^{[k]}$ and $\phi_l^{[k]}$, respectively, as is shown in Fig. 2. Moreover, since each of the M photodiodes of the user k is characterized by a distinct orientation, there exist M , $m = \{1, \dots, M\}$, possible incidence angles per user¹. Thus, the LoS component is given by [10]

$$\eta_{\text{LoS}, l}^{[k]}(m) = \begin{cases} \frac{\gamma A}{d_{kl}^2} R_0(\phi_l^{[k]}) T(\phi_l^{[k]}(m)) \cos(\phi_l^{[k]}(m)) & \text{if } \phi_l^{[k]}(m) \leq \Psi_c \\ 0 & \text{if } \phi_l^{[k]}(m) \geq \Psi_c \end{cases}, \quad (9)$$

where A and γ are the area of detection and the responsivity of each photodiode, respectively, $T(\phi_l^{[k]}(m))$ is the equivalent gain of the optical filter plus concentrator and Ψ_c is the FoV of each photodiode. Moreover, in (9), R_0 represents the Lambertian radiation intensity given by $R_0 = \frac{v+1}{2\pi} \cos^v(\phi)$ where $v = \frac{-\ln 2}{\ln \cos(\phi_{1/2})}$ where $\phi_{1/2}$ is the transmitter semiangle.

Taking into consideration the delay between the LoS and NLoS components, the contribution of the NLoS component in the frequency domain is [10]

$$h_{\text{diff}}(f) = \eta_{\text{diff}} \frac{e^{j2\pi\Delta T}}{1 + j\frac{f}{f_D}} \quad (10)$$

¹The angle of irradiance between each photodiode of the user k and the transmitter l can be approximated as $\phi_l^{[k]}(m) \approx \phi_l^{[k]}$.

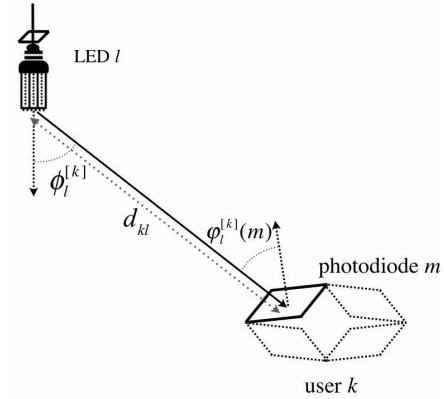


Fig. 2. Geometry of the pair transmitter-receiver for optical transmission.

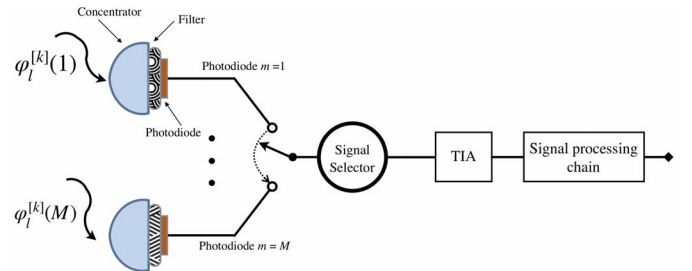


Fig. 3. Structure of the reconfigurable photodetector. Each photodiode provides a distinct incidence angle.

where f_D is the -3 dB cut-off frequency of the diffuse optical channel and $\eta_{\text{diff}} = \frac{A}{A_{\text{room}}} \frac{\rho}{1-\rho}$ represents the amount of reflected optical power where A_{room} is the area of reflection surface and ρ is the reflectivity of the area illuminated by the optical transmitter.

Therefore, the channel impulse response in the frequency domain is

$$h_l^{[k]}(m, f) = \eta_{\text{LoS}, l}^{[k]}(m) + h_{\text{diff}}(f). \quad (11)$$

It can be seen that the LoS component depends on the incidence angle, and therefore, on the preset mode associated to the preset mode m . Moreover, for modulation bandwidths below the cut-off frequency f_D the NLoS component provides a constant contribution independently of the orientation of each photodiode, i.e., its incidence angle.

C. Reconfigurable photodetector

In this work, we focus on the concept of reconfigurable photodetector proposed in [8]. Basically, a reconfigurable photodetector is composed of a set of photodiodes connected to a single signal processing chain as is shown in Fig. 3. Notice that this structure only requires a single transimpedance amplifier (TIA), which reduces considerably the power consumption of the receiver. We consider a pyramidal arrangement in which all the photodiodes are characterized by the same azimuthal angle denoted as θ_{pyr} while the polar angle of the photodiode m of the user k is given by $\alpha^{[k,m]} = \frac{2(m-1)\pi}{L}$, $m = \{1, \dots, M\}$. However, other arrangements such as a hemispherical distribution can be proposed [6].

Taking into consideration the L transmitters of the network and reconfigurable photodetectors providing M preset modes each, the resulting channel matrix of the user k is

$$\mathbf{H}^{[k]} = \begin{bmatrix} \mathbf{h}^{[k]}(1)^T \\ \mathbf{h}^{[k]}(2)^T \\ \vdots \\ \mathbf{h}^{[k]}(M)^T \end{bmatrix} = \begin{bmatrix} h_1^{[k]}(1) & h_2^{[k]}(1) & \dots & h_L^{[k]}(1) \\ h_1^{[k]}(2) & h_2^{[k]}(2) & \dots & h_L^{[k]}(2) \\ \vdots & \vdots & \ddots & \vdots \\ h_1^{[k]}(M) & h_2^{[k]}(M) & \dots & h_L^{[k]}(M) \end{bmatrix}. \quad (12)$$

It is interesting to remark that the goal of the reconfigurable photodetector is to provide linearly independent channel responses regarding each preset mode.

V. MEASUREMENT SET-UP

We consider two LED lights as described in Section IV-A deployed as is shown in Fig. 4. The optical transmitters and receivers are located in a laboratory of the Universidad Carlos III de Madrid. Due to the space limitations in the laboratory, we consider a distance between transmitter and receiver of $d_{\text{user}} = 1.5$ m while the distance between optical transmitters is $d_{\text{LED}} = 50$ cm. Moreover, the drive current of the lights is limited to 200 mA, which generates an optical power of 5 W, for the safety of the human eyes. However, this scheme can be extended to a higher distance case considering higher drive current for the LED lights.

In order to evaluate the performance of the reconfigurable photodetector we consider a structure as is shown in Fig. 5 in which the receiver is composed of $M = 4$ photodiodes following a pyramidal pattern. We first consider a PIN photodiode Osram SFH203 [11] with a FoV equivalent to $\pm 25^\circ$. Thus, considering an incidence angle of $\{0, 15, 30, 45, 90\}$, the resulting channel matrix for a user located in front of the transmitter $l = 1$ (see Fig. 4) is

$$\tilde{\mathbf{H}} = \begin{bmatrix} \tilde{\mathbf{h}}_1 \\ \tilde{\mathbf{h}}_2 \end{bmatrix}^T = \begin{bmatrix} 0.832 & 0.506 & 0.199 & 0.108 & 0 \\ 0.149 & 0.417 & 0.668 & 0.596 & 0.137 \end{bmatrix}^T \quad (13)$$

where $\tilde{\mathbf{h}}_l = \frac{\mathbf{h}_l^T}{\|\mathbf{h}_l\|}$ is the normalized vector of the channel response between the transmitter l and the considered user for the $M = 5$ preset modes, which are given by the incidence angle. Obtaining the determinant of the pseudoinverse of the channel matrix, i.e., $\det(\tilde{\mathbf{H}}\tilde{\mathbf{H}}^H)$, we obtain a value equal to 0.72. Therefore, we can conclude that the channel entries between the transmitter 1 and 2 are considerably uncorrelated. Furthermore, notice that the channel component obtained for an incidence angle of 90° purely corresponds to the diffuse component. For the considered photodiode model it only provides a detectable value for the transmitter 2, i.e., the nearest to the wall. However, even in this case the channel component is much lower than for other incidence angles.

The same procedure is carried out considering the photodiode Vishay BPW21 [12], which is characterized by a larger area of detection and a wide FoV of $\pm 50^\circ$. In this case, the resulting normalized channel matrix is

$$\tilde{\mathbf{H}} = \begin{bmatrix} \tilde{\mathbf{h}}_1 \\ \tilde{\mathbf{h}}_2 \end{bmatrix}^T = \begin{bmatrix} 0.510 & 0.479 & 0.457 & 0.425 & 0.106 \\ 0.350 & 0.432 & 0.458 & 0.447 & 0.319 \end{bmatrix}^T. \quad (14)$$

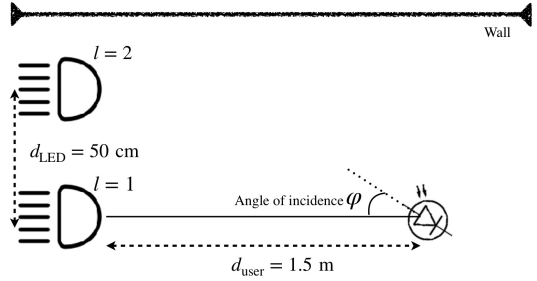


Fig. 4. Measurement set-up.

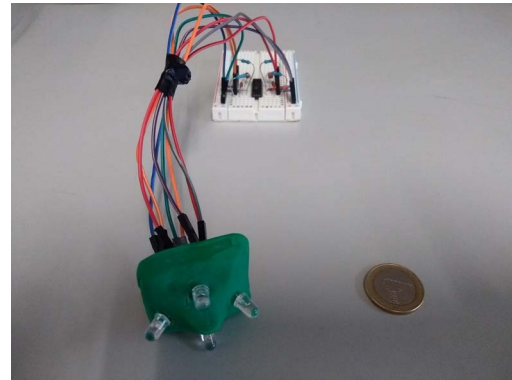


Fig. 5. Reconfigurable photodetector employed for the channel measurement.

In this case, it can be seen that the channel response barely varies regarding the incidence angle. Indeed, $\det(\tilde{\mathbf{H}}\tilde{\mathbf{H}}^H) = 0.026$ for the channel matrix (14). However, it can be seen that the considered photodiodes provide a constant channel even considering only the diffuse contribution. Therefore, photodiodes characterized by a wide FoV are complementary to narrow FoV photodiodes. That is, a receiver can consider both approaches for distinct purposes.

VI. RESULTS AND OFF-LINE EVALUATION

First, we analyze the correlation among the channel responses provided by the proposed reconfigurable photodetector. In this sense, we define the following evaluation matrix

$$\mathbf{H}_{\text{eval}} = \begin{bmatrix} h_1^{[k]}(\varphi = 0^\circ) & h_2^{[k]}(\varphi = 0^\circ) \\ h_1^{[k]}(\varphi) & h_2^{[k]}(\varphi) \end{bmatrix}, \quad (15)$$

where the first preset mode is fixed to $\varphi = 0^\circ$ while the second preset mode varies among distinct incidence angles. The evolution of $\det(\mathbf{H}_{\text{eval}}\mathbf{H}_{\text{eval}}^H)$ is plotted in Fig. 6. It can be seen that the channel responses are totally correlated considering photodiodes pointing to the same orientation. Hence, BIA schemes cannot be implemented without considering a reconfigurable photodetector based on AD arrangement of photodiodes. Using the photodiodes SFH203, it can be seen that the channel responses are uncorrelated for the range of incidence angles between the FoV. Moreover, as the incidence angle increases out of the FoV range only the diffuse component is considered. In this sense, it can be seen that the diffuse component provides correlated channel responses. Considering the photodiode BPW21 the channel responses

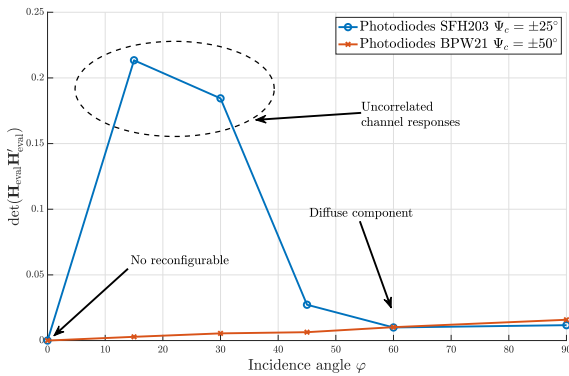


Fig. 6. Correlation of the channel responses for distinct incidence angles.

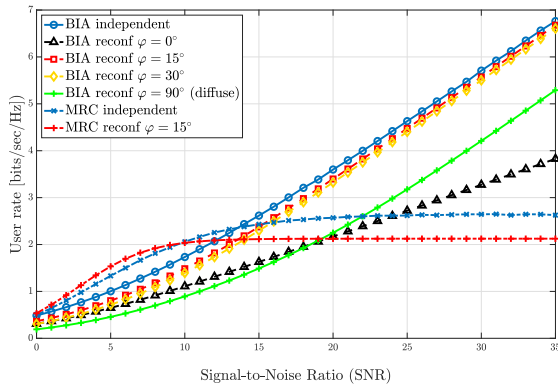


Fig. 7. Achievable user rate for BIA and comparison with MRC considering independent channel responses and the channel obtained for the proposed reconfigurable photodetector.

are considerably correlated. In this case, the goal of the reconfigurable photodetector cannot be satisfied considering photodiodes with features similar as the BPW21, i.e., wide FoV and flat radiation sensitivity.

In Fig. 7 we show an off-line evaluation of the user rate achieved by BIA and MRC considering the normalized channel obtained by the proposed reconfigurable photodetector based on the SFH203 photodiode. For comparison purposes, we first evaluate the user rate of BIA considering independent and correlated responses. It can be seen that correlated responses, i.e., photodiodes pointing to the same orientation, penalizes considerably the performance of BIA. Indeed, notice that the slope of the user rate for this case indicates the penalty in multiplexing gain. For the reconfigurable photodetector, the difference between the incidence angles generates a user rate close to the obtained by the independent channel response. Comparing with a diversity scheme such as MRC, which also exploits the architecture of the AD receiver, the user rate is limited by the interference mitigation. That is, for a SNR greater than 10 dB the user rate is limited by interference while the BIA scheme increases the achievable rate beyond this point. Interestingly, a similar behaviour occurs between IA based on MMSE receivers [13].

VII. CONCLUSIONS

In this work, we present an evaluation of the reconfigurable photodetector, which is proposed for the implementation of BIA schemes in vehicular communications based on VLC. It is shown that the reconfigurable photodetector provides linearly independent channel responses considering photodiodes with a narrow FoV and a selective sensitivity pattern. However, photodiodes with wide FoV lead to correlated channel responses independently of the angle of incidence. Thus, considering a reconfigurable photodetector composed of proper photodiodes following an angle diversity distribution, it is demonstrated that the performance of BIA is close to the obtained for independent channel responses. Furthermore, it is shown that BIA outperforms the rate achieved by MRC schemes for VLC. Further works consider an evaluation over-the-air of BIA considering a mechanical system for selecting the receiving orientation angle of each user, i.e., its preset mode.

REFERENCES

- [1] P. H. Pathak, X. Feng, P. Hu, and P. Mohapatra, "Visible light communication, networking, and sensing: A survey, potential and challenges," *IEEE Communications Surveys Tutorials*, vol. 17, no. 4, pp. 2047–2077, Fourthquarter 2015.
- [2] A. Cailean and M. Dimian, "Current challenges for visible light communications usage in vehicle applications: A survey," *IEEE Communications Surveys Tutorials*, vol. 19, no. 4, pp. 2681–2703, Fourthquarter 2017.
- [3] A. Cailean, B. Cagneau, L. Chassagne, V. Popa, and M. Dimian, "A survey on the usage of dsrc and vlc in communication-based vehicle safety applications," in *2014 IEEE 21st Symposium on Communications and Vehicular Technology in the Benelux (SCVT)*, Nov 2014, pp. 69–74.
- [4] M. Yasir, S. Ho, and B. N. Vellambi, "Indoor position tracking using multiple optical receivers," *Journal of Lightwave Technology*, vol. 34, no. 4, pp. 1166–1176, Feb 2016.
- [5] Z. Chen, D. A. Basnayaka, X. Wu, and H. Haas, "Interference mitigation for indoor optical attocell networks using an angle diversity receiver," *Journal of Lightwave Technology*, vol. 36, no. 18, pp. 3866–3881, Sep. 2018.
- [6] A. Nuwanpriya, S. Ho, and C. S. Chen, "Indoor mimo visible light communications: Novel angle diversity receivers for mobile users," *IEEE Journal on Selected Areas in Communications*, vol. 33, no. 9, pp. 1780–1792, Sep. 2015.
- [7] T. Gou, C. Wang, and S. A. Jafar, "Aiming perfectly in the dark-blind interference alignment through staggered antenna switching," *IEEE Trans. on Sig. Proc.*, vol. 59, no. 6, pp. 2734–2744, June 2011.
- [8] M. Morales-Céspedes, M. C. Paredes-Paredes, A. García Armada, and L. Vandendorpe, "Aligning the light without channel state information for visible light communications," *IEEE Journal on Selected Areas in Communications*, vol. 36, no. 1, pp. 91–105, Jan 2018.
- [9] "CitiLed COB Series CLU04848-1212C4," Citizen, Datasheet, 2019. [Online]. Available: <https://bit.ly/2EryDsV>
- [10] V. Jungnickel, V. Pohl, S. Nonnig, and C. von Helmolt, "A physical model of the wireless infrared communication channel," *IEEE J. on Selected Areas in Comm.*, vol. 20, no. 3, pp. 631–640, April 2002.
- [11] "Radial T1 3/4, SFH 203," Osram Opto Semiconductors, Datasheet, 2019. [Online]. Available: <https://bit.ly/2VFhfbk>
- [12] "BPW21R Datasheet," Vishay Semiconductors, Datasheet, 2019. [Online]. Available: <https://www.vishay.com/docs/81519/bpw21r.pdf>
- [13] J. Fanjul and I. Santamaría, "Flexible duplexing for maximum downlink rate in multi-tier mimo networks," in *2018 26th Telecommunications Forum (TELFOR)*, Nov 2018, pp. 1–6.